Suppressing neutrophil-dependent angiogenesis abrogates resistance to anti-VEGF antibody in a genetic model of colorectal cancer

Yoshiro Itatani[a,b,1], Takamasa Yamamoto[a,1], Cuiling Zhong[a], Alfredo A. Molinolo[a], Jane Ruppel[c], Priti Hegde[c,2], M. Mark Taketo[d], and Napoleone Ferrara[a,3]

[a]Moores Cancer Center, University of California San Diego, La Jolla, CA 92093; [b]Department of Surgery, Graduate School of Medicine, Kyoto University, Sakyo, 606-8501 Kyoto, Japan; [c]Bioanalytical Sciences Department, Genentech, Inc., South San Francisco, CA 94080; and [d]Division of Experimental Therapeutics, Graduate School of Medicine, Kyoto University, Sakyo, 606-8501 Kyoto, Japan

Contributed by Napoleone Ferrara, July 1, 2020 (sent for review April 30, 2020; reviewed by Raymond N. DuBois and Sanford D. Markowitz)

We tested *cis-Apc$^{\Delta 716}$/Smad4$^{+/-}$* and *cis-Apc$^{\Delta 716}$/Smad4$^{+/-}$ Kras^{G12D}* mice, which recapitulate key genetic abnormalities accumulating during colorectal cancer (CRC) tumorigenesis in humans, for responsiveness to anti-VEGF therapy. We found that even tumors in *cis-Apc$^{\Delta 716}$/Smad4$^{+/-}$ Kras^{G12D}* mice, although highly aggressive, were suppressed by anti-VEGF treatment. We tested the hypothesis that inflammation, a major risk factor and trigger for CRC, may affect responsiveness to anti-VEGF. Chemically induced colitis (CIC) in *cis-Apc$^{\Delta 716}$/Smad4$^{+/-}$* and *cis-Apc$^{\Delta 716}$/Smad4$^{+/-}$ Kras^{G12D}* mice promoted development of colon tumors that were largely resistant to anti-VEGF treatment. The myeloid growth factor G-CSF was markedly increased in the serum after induction of colitis. Antibodies blocking G-CSF, or its target Bv8/PROK2, suppressed tumor progression and myeloid cell infiltration when combined with anti-VEGF in CIC-associated CRC and in anti-VEGF-resistant CRC liver metastasis models. In a series of CRC specimens, tumor-infiltrating neutrophils strongly expressed Bv8/PROK2. CRC patients had significantly higher plasma Bv8/PROK2 levels than healthy volunteers and high plasma Bv8/PROK2 levels were inversely correlated with overall survival. Our findings establish Bv8/PROK2 as a translational target in CRC, in combination with anti-VEGF agents.

colorectal cancer | angiogenesis | inflammation | myeloid cells | drug resistance

Antiangiogenesis represents a validated therapeutic strategy for a variety of disorders. The anti-vascular endothelial growth factor (VEGF)-A monoclonal antibody (Mab), bevacizumab (Avastin) was first approved by the Food and Drug Administration (FDA) for treatment of metastatic colorectal cancer (CRC) in February 2004 and was subsequently approved for several additional solid tumor types and currently ranks among the most widely used cancer therapeutics (1). In addition to the anti-VEGF-A Mab, other inhibitors of the VEGF pathway, including several small molecule tyrosine kinase inhibitors, a chimeric soluble receptor, and an anti-VEGFR2 antibody, have been approved for cancer therapy (1–3). In early studies, bevacizumab was shown to confer a significant survival advantage on patients with previously untreated metastatic CRC, when combined with fluoropyrimidine-based chemotherapy (4). In addition to first-line (4) and bevacizumab-naïve second-line treatment (5), maintenance of VEGF inhibition with bevacizumab plus second-line chemotherapy has clinical benefits also for patients with metastatic CRC that progressed on bevacizumab treatment (6). Although bevacizumab results in overall survival benefits, some patients have little or no response. This primary or de novo treatment resistance is a problem common to many oncological treatments, including the most recent therapies (2).

Resistance to anti-VEGF therapy is often attributed to angiogenic escape, potentially through activation of alternative proangiogenic pathways or blood vessel cooption (3). Angiogenic factors include, besides VEGF-A, acidic and basic fibroblast growth factor (aFGF and bFGF), placenta growth factor (PlGF), VEGF-C, hepatocyte growth factor (HGF), platelet-derived growth factors (PDGFs), the Tie-2 ligands Angiopoietin (Ang)-1, Ang-2, etc. (7, 8).

Unfortunately, despite promising preclinical studies, attempts at improving outcomes of anti-VEGF therapy in CRC patients through combination with agents targeting Ang-2, the HGF receptor cMet, EGFL7, the Hedgehog pathway, or by stimulating the extrinsic apoptotic pathway with Apo2L/tumor necrosis factor-related apoptosis-inducing ligand (TRAIL), so far have not been met with success as reviewed in refs. 2, 3. Therefore, the key mechanisms of resistance/relapse to anti-VEGF agents in the clinical setting remain largely unknown.

The tumor microenvironment is a complex system comprised of several cell types, including vascular endothelial cells, fibroblasts, and immune cells. The cellular composition of the microenvironment

Significance

Using mouse models that recapitulate key genetic abnormalities accumulating during colorectal cancer (CRC) tumorigenesis, we report that chemically induced colitis promoted development of colon tumors that were largely resistant to anti-VEGF antibody treatment. Serum G-CSF levels were markedly elevated after induction of colitis. Inhibition of G-CSF or Bv8/PROK2 increased the efficacy of anti-VEGF antibody and prevented onset of resistance. To verify the potential clinical relevance of these findings, we examined a series of CRC specimens and found that tumor-infiltrating neutrophils strongly expressed Bv8/PROK2. CRC patients had significantly higher plasma Bv8/PROK2 levels than healthy volunteers and high plasma Bv8/PROK2 levels were inversely correlated with overall survival. These findings establish Bv8/PROK2 as a translational target in CRC, in combination with anti-VEGF agents.

Author contributions: Y.I., T.Y., P.H., and N.F. designed research; Y.I., T.Y., C.Z., J.R., and P.H. performed research; M.M.T. contributed new reagents/analytic tools; Y.I., T.Y., C.Z., A.A.M., P.H., and N.F. analyzed data; and Y.I., T.Y., and N.F. wrote the paper.

Reviewers: R.N.D., Medical University of South Carolina; and S.D.M., Case Western Reserve University.

Competing interest statement: J.R. is an employee of Genentech, Inc. P.H. is a former employee of Genentech, Inc. and a current employee of Foundation Medicine, Inc.

[1]Y.I. and T.Y. contributed equally to this work.

[2]Present address: Foundation Medicine, Inc., Cambridge, MA 02141.

[3]To whom correspondence may be addressed. Email: nferrara@ucsd.edu.

This article contains supporting information online at https://www.pnas.org/lookup/suppl/doi:10.1073/pnas.2008112117/-/DCSupplemental.

First published August 19, 2020.

is tumor specific and may profoundly affect therapeutic responses to anticancer agents (9). Indeed, the various cell types communicate through cytokine/chemokine networks that may suppress or promote tumor progression (10). In CRC, it has been proposed that the density of infiltrating lymphocytes inside tumor tissues or "immune score" can predict clinical outcomes (11). These findings led to the hypothesis that activating T cell function by blocking programmed death ligand 1 (PD-L1) or programmed death 1 (PD-1) signaling may be an effective treatment for advanced CRC patients. However, studies with anti-PD-L1 or PD-1 antibodies so far have not demonstrated significant benefit to CRC patients, although these agents conferred durable benefits on subsets of patients with other solid tumor types (12). Recently, it was reported that microsatellite instability (MSI) in CRC predicts responses to immunotherapy (13). However, MSI-high patients account for only 15% of total CRC patients (14).

Here we report that treatment with an anti-VEGF antibody significantly suppressed tumor angiogenesis and growth in mice harboring key genetic mutations associated with human intestinal cancer. Since inflammation is involved in sporadic and heritable CRC, as well as in ulcerative colitis-associated cancers (15), we tested the hypothesis that colitis may affect responsiveness to anti-VEGF. Indeed, chemically induced colitis (CIC) caused by dextran sulfate sodium (DSS) promoted the development of colonic tumors that were largely unresponsive to anti-VEGF antibody, although small intestinal tumors in the same animal were still responsive. We sought to dissect the mechanisms of such resistance to anti-VEGF therapy.

Results

Anti-VEGF Treatment Suppresses Tumor Formation and Prolongs Survival in Intestinal Cancer Genetically Engineered Mouse Models (GEMMs). It has been reported that treatment with an anti-VEGF antibody suppresses tumor growth and prolongs survival of adenomatous polyposis coli $(Apc)^{+/min}$ mice (16), which carry a heterozygous truncation allele at codon 850 of Apc and serve as a model of familial adenomatous polyposis (FAP) (17). However, these findings do not predict whether malignant cancer responds to anti-VEGF antibody treatment because *Apc* mutations alone lead to benign adenomas with few malignant adenocarcinomas (18). Namely, additional mutations in *Kras*, *p53*, or loss of heterozygosity at chromosome 18q (including *Smad2/4*) appear to be involved in adenoma-carcinoma progression. To determine whether the cross-species reactive anti-VEGF-A neutralizing monoclonal antibody B20-4.1 (19) (anti-VEGF hereafter) has inhibitory effects on intestinal cancer, we took advantage of a GEMM carrying *cis*-compound mutations in *Apc* and *Smad4* (*cis-Apc/Smad4*) that develops spontaneous invasive intestinal cancers (18), compared with the intestinal adenoma model with $Apc^{\Delta 716}$ mutation.

In agreement with earlier findings (16), tumor formation and growth were significantly suppressed in $Apc^{\Delta 716}$ mice treated with anti-VEGF (tumor numbers 7.6 ± 2.6 vs. 13.4 ± 2.2, $P < 0.01$; tumor area, 3.8 ± 1.6 vs. 28.7 ± 11.5 [mm^2], $P < 0.01$, Student's *t* test) (*SI Appendix*, Fig. S1 *A–D*). Tumor growth was also suppressed in *cis-Apc/Smad4* mice (Fig. 1 *A* and *B* and *SI Appendix*, Fig. S1*E*). Namely, when *cis-Apc/Smad4* mice were treated with anti-VEGF for 6 wk or 9 wk from 13 wk old on, both tumor numbers and total tumor areas were significantly reduced (tumor number of 6-wk treatment 14.1 ± 4.2 vs. 17.7 ± 2.8, $P < 0.05$; tumor area of 6-wk treatment, 8.9 ± 3.6 vs. 69.8 ± 25.9 [mm^2], $P < 0.01$; tumor numbers of 9-wk treatment 12.0 ± 3.9 vs. 21.4 ± 9.1, $P < 0.05$; tumor area of 9-wk treatment, 9.1 ± 5.0 vs. 91.3 ± 38.9 [mm^2], $P < 0.01$, Student's *t* test) (Fig. 1*B*). Mice with intestinal tumors showed pale paws due to anemia caused by mucosal bleeding, which often resulted in death. Anti-VEGF maintained hematocrit levels in a normal range (6-wk treatment 54.3 ± 2.9 vs. 35.0 ± 8.3 [%], $P < 0.01$; 9-wk treatment 57.3 ± 2.6 vs. 30.3 ± 4.0 [%], $P < 0.01$, Student's *t* test) (*SI Appendix*, Fig. S1*F*). Anti-VEGF also suppressed tumor invasion and progression in tumor malignancy grades (Fig. 1*C*). Moreover, anti-VEGF improved mouse survival in a dose-dependent manner (isotype IgG 186 ± 11.9, anti-VEGF 10 mg/kg/week 250 ± 18.4, anti-VEGF 20 mg/kg/week 333 ± 24.4 [days], $P < 0.01$, log-rank test) (Fig. 1*D*).

We also added an oncogenic *Kras* mutation G12D, controlled by loxP stop cassette ($LSL\text{-}Kras^{G12D/+}$) (20) and *villin-Cre* transgene (21) to the *cis-Apc/Smad4* mutation mice (*cis-Apc/Smad4* $Kras^{G12D(villin)}$). Expression of intestinal epithelial cell-specific Cre in *villin-Cre* mice was confirmed by mating with $Gt(ROSA26)^{ACTB\text{-}tdTomato\text{-}EGFP}$ mice (*SI Appendix*, Fig. S2 *A* and *B*). As anticipated, *cis-Apc/Smad4* $Kras^{G12D(villin)}$ mice had a short lifetime of about 8 to 14 wk after birth, due to highly invasive intestinal tumors (*SI Appendix*, Fig. S2*C*). Nevertheless, *cis-Apc/Smad4* $Kras^{G12D(villin)}$ mice treated with anti-VEGF had smaller tumor areas (40.7 ± 23.2 vs. 79.1 ± 22.2 [mm^2], $P < 0.01$, Student's *t* test), showed longer survival (95.0 ± 3.3 vs. 73.0 ± 4.3 [days], $P < 0.01$, log-rank test), and the tumors were less invasive, although tumor numbers were not much affected (29.0 ± 13.6 vs. 35.0 ± 11.8, $P = 0.33$) (Fig. 1 *E–G*). Collectively, these results indicated that anti-VEGF treatment suppressed tumor growth and invasion in mouse models for spontaneous intestinal cancer, leading to increased survival.

Colorectal Tumors Associated with CIC in *cis-Apc/Smad4* and *cis-Apc/Smad4* $Kras^{G12D(CDX2)}$ Mice Are Resistant to Anti-VEGF Therapy. Inflammation is one of the key events in the pathogenesis of cancer (22) and CRC is strongly associated with inflammation (15). Although polyps in patients with hereditary CRC such as FAP or Lynch syndrome rarely show clear signs of chronic inflammation, tumorigenesis can be prevented or suppressed by long-term administration of antiinflammatory drugs (23). It has been reported that CIC induced by short-term DSS feeding causes colorectal tumor formation in $Apc^{+/min}$ mice (24). *Cis-Apc/Smad4* mutant mice, as well as $Apc^{\Delta 716}$ mice, also showed tumor formation in the colorectum after only 1-wk administration of DSS (tumor number 11.1 ± 5.0 vs. 1.5 ± 0.8, $P < 0.01$; tumor area 86.8 ± 40.0 vs. 12.9 ± 7.8 [mm^2], $P < 0.01$, Student's *t* test) (Fig. 2 *A–C* and *SI Appendix*, Fig. S3*A*), which recapitulated invasive human CRC with *Apc* and *Smad4* mutations (Fig. 2*D* and *SI Appendix*, Fig. S3 *C* and *D*). In this model, we did not observe any differences in tumor formation in the small intestine (tumor number 16.5 ± 6.1 vs. 16.5 ± 3.4, $P = 0.62$; tumor area 35.7 ± 22.6 vs. 56.9 ± 26.8 [mm^2], $P = 0.07$, Student's *t* test) (Fig. 2*C*). We treated *cis-Apc/Smad4* mice with anti-VEGF for 6 wk following the induction of colorectal tumors with DSS, and found that they were refractory to anti-VEGF treatment (tumor number 9.5 ± 4.1 vs. 11.1 ± 5.0, $P = 0.45$; tumor area 66.0 ± 40.2 vs. 86.8 ± 39.8 [mm^2], $P = 0.25$, Student's *t* test) (Fig. 2*C*). On the other hand, small intestinal tumors still responded even after DSS feeding (tumor area 13.6 ± 7.6 vs. 35.7 ± 22.6 [mm^2], $P < 0.01$, Student's *t* test) (Fig. 2*C*). Since we could not design the DSS feeding in *cis-Apc/Smad4* $Kras^{G12D(villin)}$ mice due to their short lifespan of 100 d or less, we bred mice carrying $CDX2P\text{-}CreER^{T2}$ transgene (25) instead of *villin-Cre* in order to induce Cre activation by tamoxifen administration (4 consecutive days at 9 wk of age intraperitoneally) only in colorectal epithelial cells (*SI Appendix*, Fig. S2 *A* and *B*) and added it to *cis-Apc/Smad4* mice to generate *cis-Apc/Smad4* $Kras^{G12D(CDX2)}$ mice. DSS administration following Cre activation by tamoxifen significantly promoted colorectal tumor formation in *cis-Apc/Smad4* $Kras^{G12D(CDX2)}$ mice (Fig. 2 *A–C* and *SI Appendix*, Fig. S3*E*). We treated *cis-Apc/Smad4* $Kras^{G12D(CDX2)}$ mice with anti-VEGF for 3 wk following the induction of colorectal tumors with tamoxifen and DSS and found that they were refractory to anti-VEGF treatment as well (tumor area 281 ± 40 vs. 242 ± 63 [mm^2], $P = 0.21$, Student's *t* test) (Fig. 2*C*).

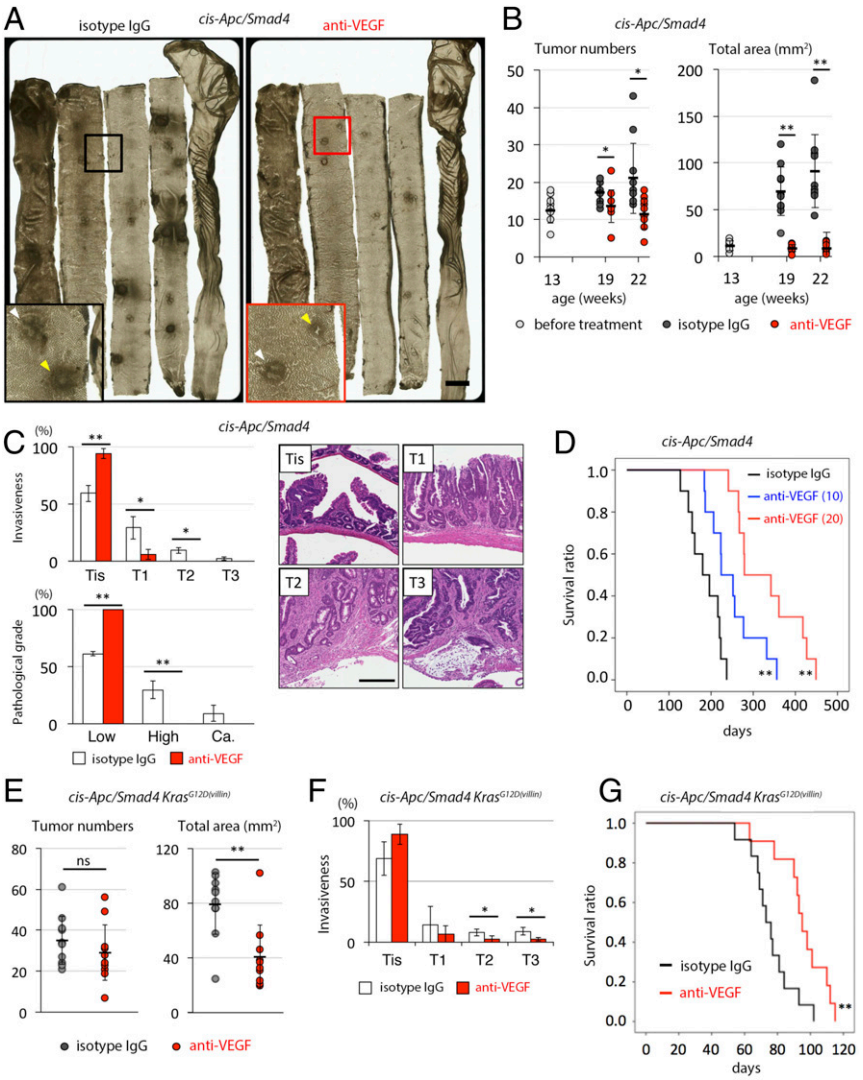

Fig. 1. Anti-VEGF antibody treatment suppressed tumor formation and prolonged survival. (*A*) Representative images of small and large intestinal sections of *cis-Apc/Smad4* mice treated with isotype IgG control or anti-VEGF antibody for 6 wk. White arrowheads, Payer's patches; yellow arrowheads, tumors. (Scale bar, 5 mm.) (*B*) Chronological changes in intestinal tumor numbers and total tumor areas in *cis-Apc/Smad4* mice treated with control or with anti-VEGF antibody. ($n = 10$ in each group. $^*P < 0.05$, $^{**}P < 0.01$, Student's *t* test). (*C*) Quantification of the depth of tumor invasion (*Left Upper*) and morphology (*Left Lower*) at age 22 wk (9-wk treatment). *Right* show representative tumors of each indicated invasion depth. $n = 3$ in each group. Tis/T1/T2/T3, TNM classification of the American Joint Committee on Cancer; low, low grade adenoma; high, high grade adenoma; Ca, adenocarcinoma. $^*P < 0.05$; $^{**}P < 0.01$, Student's *t* test. (Scale bar, 200 μm.) (*D*) Kaplan–Meier estimates of *cis-Apc/Smad4* mice treated with isotype IgG control (black line), 10 mg/kg/week of anti-VEGF (blue line), or 20 mg/kg/week of anti-VEGF (red line). $n = 10$ in each group; $^{**}P < 0.01$, log-rank test. (*E*) Quantification of tumor numbers and total tumor areas of *cis-Apc/Smad4* $Kras^{G12D(villin)}$ mice treated with isotype IgG control or anti-VEGF for 4 wk (from 6 to 9 wk old). $n = 10$ in each group; ns, not significant; $^{**}P < 0.01$, Student's *t* test. (*F*) Quantification of the depth of tumor invasion at age 10 wk after 4-wk treatment with isotype IgG control or anti-VEGF. $n = 4$ in each group; $^*P < 0.05$, Student's *t* test. (*G*) Kaplan–Meier estimates of *cis-Apc/Smad4* $Kras^{G12D(villin)}$ mice treated with isotype IgG control (black line, $n = 12$) or 20 mg/kg/week of anti-VEGF (red line, $n = 11$). $^{**}P < 0.01$, log-rank test.

Higher Serum Granulocyte-Colony Stimulating Factor (G-CSF) Levels in Mice Harboring Anti-VEGF Resistant Colorectal Tumors. To investigate the differences between the small intestinal and colorectal tumors in DSS-treated *cis-Apc/Smad4* mice, we performed immunohistochemistry (IHC) for β-Catenin and Smad4. However, both small intestinal and colorectal tumors of $Apc^{\Delta 716}$ mice showed nuclear accumulation of β-Catenin and Smad4, whereas those of *cis-Apc/Smad4* mice had only β-Catenin accumulation in the nuclei lacking Smad4 expression in tumor epithelial cells (*SI Appendix*, Fig. S3 *C* and *D*). Although it has been reported that DSS causes some inflammation in the small intestine, clearly its major effects are in the colon and rectum (26) (*SI Appendix*, Figs. S3*B* and S4*A*). Thus, we examined a panel of inflammation-related genes in the colorectal tumor tissue of DSS-treated mice as compared with small intestinal tumors, and found that most of them were indeed up-regulated (*SI Appendix*, Fig. S4*B*). We also tried to determine whether there are any differences in CIC colorectal tumors among genetic backgrounds by comparing tumor tissues from $Apc^{\Delta 716}$, *cis-Apc/Smad4*, and *cis-Apc/Smad4* $Kras^{G12D(CDX2)}$ mice treated with DSS. However, we found only minor differences in terms of inflammatory and angiogenic factor expression among the various backgrounds (*SI Appendix*, Fig. S4*C*). It is worth noting that release of cytokines/chemokines into the systemic circulation is essential for an effective communication between the tumor and bone marrow. Therefore, we compared serum cytokine profiles between DSS-treated and nontreated *cis-Apc/Smad4* mice using cytokine protein arrays (*SI Appendix*, Fig. S5 *A–D*). The results showed increased levels of

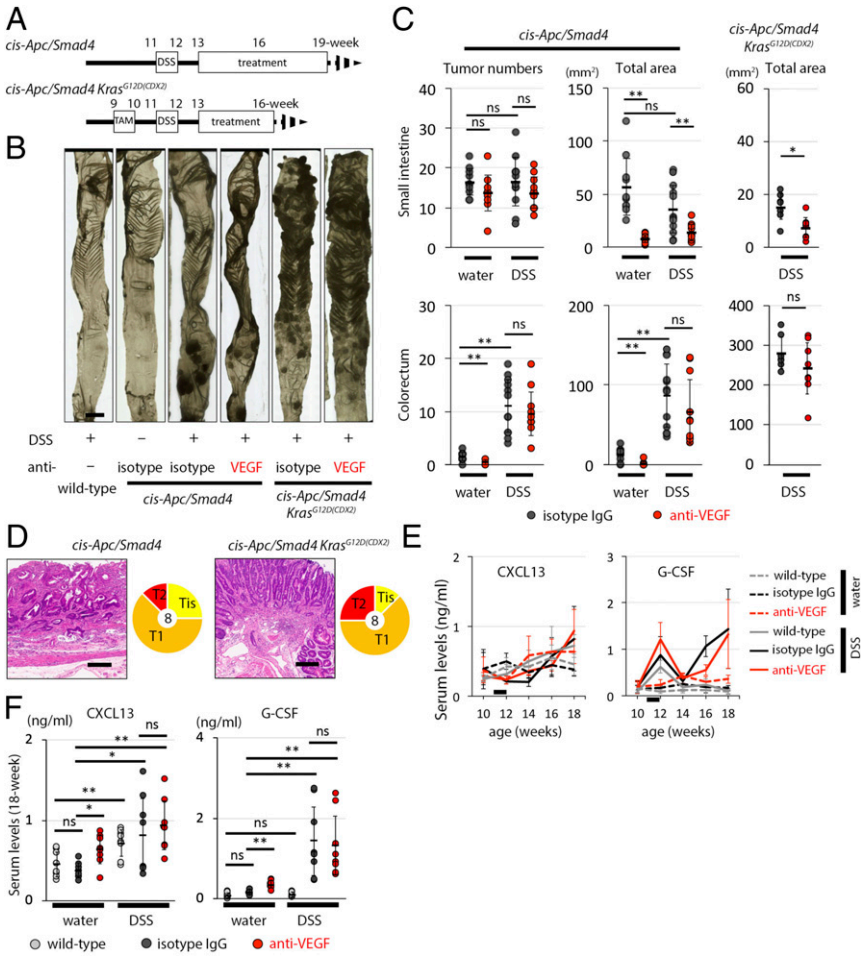

Fig. 2. DSS in drinking water promoted formation of colorectal tumors in GEMM, which were resistant to anti-VEGF treatment. (*A*) Schematic representation of DSS feeding, tamoxifen administration (2 mg in 100 μL corn oil, 4 consecutive days intraperitoneally) and anti-VEGF treatment. (*B*) Colorectum images from mice with or without DSS feeding and anti-VEGF (or isotype IgG control). (Scale bar, 5 mm.) (*C*) Comparison of tumor numbers and total tumor areas of *cis-Apc/Smad4* and *cis-Apc/Smad4 Kras*$^{G12D(CDX2)}$ mice with or without DSS feeding, followed by treatment with anti-VEGF or isotype IgG control. *Upper* show tumors in small intestine, and *Lower* show those in colorectum. $n = 10$ in each group, $^{*}P < 0.05$; $^{**}P < 0.01$. ns, not significant, Student's *t* test. (*D*) Representative images of invasive adenocarcinomas from *cis-Apc/Smad4* (*Left*) and *cis-Apc/Smad4 Kras*$^{G12D(CDX2)}$ (*Right*) with tamoxifen after CIC. (Scale bar, 5 mm.) Pie charts indicates tumor invasion ratios for each genotype. *Center* numbers indicate mice analyzed for invasion status. (*E*) Chronological changes in serum CXCL13 and G-CSF levels. Black short bars inside each graph showed the period of DSS treatment (for 1 wk at age 11 wk). $n = 5$ in each group. (*F*) Serum CXCL13 (*Left*) and G-CSF (*Right*) levels at age 18 wk of the mice with indicated treatment. $n = 8$ in each group; $^{*}P < 0.05$. $^{**}P < 0.01$; ns, not significant, Mann–Whitney *u* test.

C-X-C motif chemokine ligand (CXCL)13 and G-CSF (among 40 cytokine/chemokines) in DSS-fed mice, with or without anti-VEGF treatment. To analyze these cytokines in a more quantitative manner, we collected serum samples chronologically and performed ELISA. Serum G-CSF levels increased in a biphasic manner; shortly after DSS treatment (initial peak), and after recovery within 2 wk, they gradually increased again, coincident with colorectal tumor growth (secondary peak). The G-CSF levels in *cis-Apc/Smad4* mice were elevated significantly 6 wk after DSS feeding (water with isotype 0.16 ± 0.05, water with anti-VEGF 0.36 ± 0.09, DSS with isotype 1.42 ± 0.85, DSS with anti-VEGF 1.33 ± 0.74 [ng/mL]), whereas they stayed at the baseline in wild-type mice (water on wild-type 0.09 ± 0.05, DSS on wild-type 0.10 ± 0.06, $P = 0.66$ [Student's *t* test] and $P = 0.60$ [Mann–Whitney *u* test]) (Fig. 2 *E*, *Right* and Fig. 2 *F*, *Right*). On the other hand, CXCL13 levels did not show any transient up-regulation shortly after DSS treatment, but they increased gradually throughout the observation period (Fig. 2 *E*, *Left* and Fig. 2 *F*, *Left*). Interestingly, serum CXCL13 levels also increased even in tumor-free wild-type mice after DSS treatment (water on wild-type 0.45 ± 0.15, DSS on wild-type 0.72 ± 0.16 [ng/mL], $P < 0.01$ [Student's *t* test and Mann–Whitney *u* test]), suggesting that this change was caused by the recovery from acute colonic inflammation, rather than by the tumor growth.

G-CSF Causes Neutrophil Infiltration into Tumor Stroma to Up-Regulate Bv8/Prokineticin 2 (PROK2) and Promote Angiogenesis in Colorectal Tumors Refractory to Anti-VEGF Antibody. Next we tried to determine the source(s) of G-CSF and CXCL13. We determined their mRNA levels in the colon tumors and adjacent normal tissues. *Csf3* (encoding G-CSF) and its receptor *Csf3r* were up-regulated dramatically in colorectal tumor tissues from *cis-Apc/Smad4* mice treated with DSS (Fig. 3*A*). On the other hand, *Cxcl13* and its receptor *Cxcr5* were expressed mainly in the normal colon tissues (Fig. 3*A*).

Among the cytokines that are highly expressed in colorectal tumors of DSS-treated *cis-Apc/Smad4* mice (*SI Appendix*, Fig. S4*B*), IL17a is known to stimulate G-CSF expression in the tumor microenvironment (27). Taking advantage of a recently described method (28), we cultured colorectal cancer stem cells

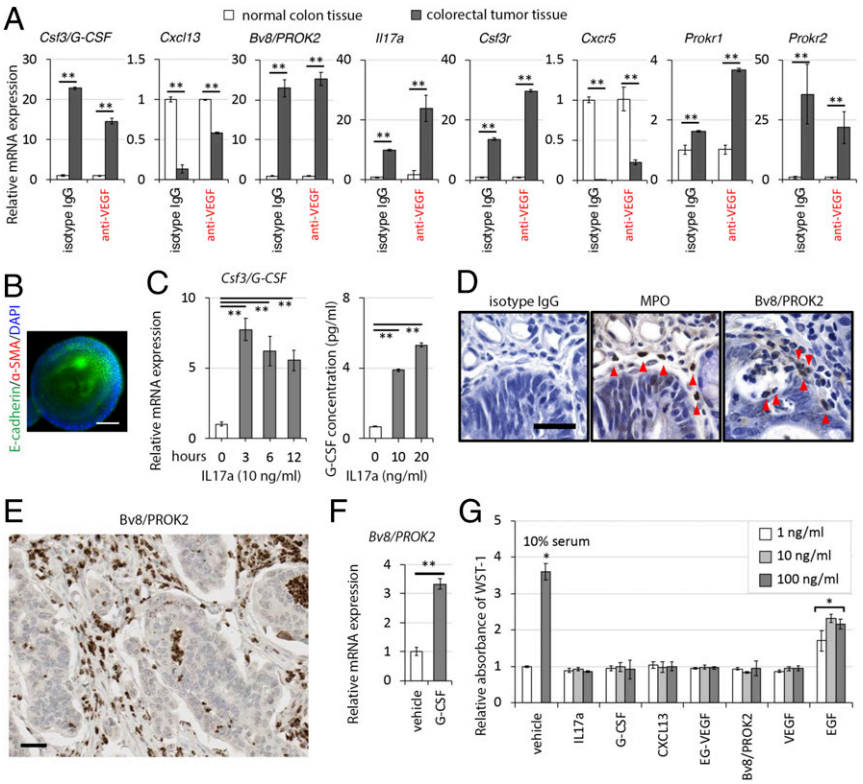

Fig. 3. G-CSF mRNA was expressed in tumor tissues, but G-CSF does not directly affect tumor cell growth. (*A*) Relative mRNA expression of *Csf3*/*G-CSF*, its receptor *Csf3r*, *Cxcl13*, its receptor *Cxcr5*, *Bv8*/*PROK2*, its receptors *Prokr1* and *Prokr2,* and *Il17a*. mRNA was collected from colorectal tumor and adjacent normal colon tissues of DSS-treated mice, with or without anti-VEGF treatment. Experiments were repeated three times. $^{**}P < 0.01$, Student's *t* test. (*B*) Immunocytostaining of primary spheroid culture cells from colorectal tumors of DSS-fed mice. All spheroid cells expressed E-cadherin, whereas no cells expressed α-SMA. (Scale bar, 50 μm.) (*C*) *Csf3*/*G-CSF* mRNA expression and its protein expression from tumor spheroid culture. Experiments were repeated three times. $^{**}P < 0.01$, Student's *t* test. (*D*) IHC for Bv8/PROK2 and MPO in tumor tissues of *cis-Apc*/*Smad4* mice with DSS. Red arrowheads, polynuclear neutrophils. (Scale bar, 50 μm.) (*E*) A representative "score 3" (see also *SI Appendix*, Fig. S6*G*) Bv8/PROK2 IHC from a human CRC specimen. (Scale bar, 40 μm.) (*F*) Relative expression of *Bv8*/*PROK2* mRNA from peripheral neutrophils with or without treatment with 10 ng/mL of G-CSF for 4 h in Hank's balanced salt solution (HBSS) buffer with 0.5% bovine serum albumin (BSA). Experiments were repeated three times. Triplicate experiments, repeated three times. $^{**}P < 0.01$, Student's *t* test. (*G*) Cell proliferation assay (WST-1 reagent) in primary spheroid cells from colorectal tumors of DSS-treated mice. Fetal bovine serum and EGF were used as positive controls. Experiments were repeated three times; $^{*}P < 0.05$, Student's *t* test.

as spheroids and treated them with recombinant IL17a (Fig. 3 *B* and *C*). Both mRNA and protein levels of G-CSF were significantly up-regulated in the IL17a-treated colorectal tumor spheroids (Fig. 3*C*). These results suggest that IL17a induced in the tumor microenvironment may stimulate G-CSF production in colorectal tumor cells.

We previously reported that Bv8/PROK2 is expressed in $CD11b^{+}Gr\text{-}1^{+}$ myeloid cells, and that it regulates myeloid cell-dependent tumor angiogenesis (29). In the present study, we found that *Bv8*/*PROK2* and its receptors *Prokr1* and *Prokr2* (30) were also highly up-regulated in the colorectal tumor tissues of DSS-treated *cis-Apc*/*Smad4* mice (Fig. 3*A*), suggesting that G-CSF from colorectal tumors stimulated production of *Bv8*/*PROK2* within the tumor. In order to confirm expression of Bv8/PROK2 within the colorectal tumor tissues, we performed immunohistochemistry for Bv8/PROK2 and myeloperoxidase (MPO). We found that polynuclear granulocytes in the tumors of DSS-treated mice expressed both antigens (Fig. 3*D* and *SI Appendix*, Fig. S6*A*), as well as human CRC tissues (Fig. 3*E*), consistent with the finding that tumor tissues had higher expression of *Bv8*/*PROK2* mRNA compared with adjacent normal tissue (Fig. 3*A*). To further validate Bv8/PROK2 expression in granulocytes/neutrophils, we isolated peripheral neutrophils from tumor-bearing mice with anti-Ly-6G beads (*SI Appendix*, Fig. S6*B*), and treated them with recombinant mouse G-CSF. After stimulation with 10 ng/mL G-CSF, peripheral neutrophils from DSS-treated *cis-Apc*/*Smad4* mice showed significant up-regulation of *Bv8*/*PROK2* expression (Fig. 3*F*). We also tested the possibility that the molecules that we targeted may have direct effects on tumor cell proliferation, we incubated tumor spheroids with IL17a, G-CSF, CXCL13, Bv8/PROK2, endocrine gland-derived vascular endothelial growth factor (EG-VEGF) (structurally related to Bv8/PROK2) or VEGF-A and found that none of these molecules had stimulatory effects (Fig. 3*G*).

We next investigated whether G-CSF expression in tumor tissues affected neutrophil infiltration into the tumor stroma by immunofluorescent staining for Ly-6G (a marker of mouse neutrophils). Anti-VEGF treatment alone promoted neutrophil infiltrations into the stroma of small intestine tumors in *cis-Apc*/*Smad4* mouse, even without CIC (*SI Appendix*, Fig. S6 *C* and *E*). DSS-induced CIC dramatically recruited neutrophil infiltration into the stroma of colorectal tumors, but not in small intestinal tumors (*SI Appendix*, Fig. S6 *C* and *E*).

We determined vascular densities in CIC-associated colorectal tumors by anti-CD34 immunohistochemistry (*SI Appendix*, Fig. S6 *D* and *F*). When treated with anti-VEGF, the tumor microvessel density of mice without DSS treatment was very low. These results are consistent with those that anti-VEGF alone almost completely suppressed tumor formation of *cis-Apc*/*Smad4* mice without DSS (Fig. 1 *A* and *B*). In contrast, CIC-associated colorectal tumors contained abundant microvessels even in mice treated with anti-VEGF (*SI Appendix*, Fig. S6 *D* and *F*),

suggesting that anti-VEGF antibody alone was unable to suppress tumor angiogenesis, and that other angiogenic factors such as Bv8/PROK2 contributed to the resistance against anti-angiogenic agents in this mouse model.

Plasma Bv8/PROK2 Levels Predicted Patient Overall Survival in Human Unresectable CRC in Response to Irinotecan, 5-Fluorouracil, Leucovorin (IFL). It has been reported that serum G-CSF levels are correlated with staging in human CRC (31). In order to further validate the findings of our mouse studies, we sought to assess Bv8/PROK2 expression in human CRC specimens by IHC using tissue microarrays (Fig. 3*E* and *SI Appendix*, Fig. S6*G*). IHC results were scored in the range of 0 to 3 based on the number of cells detected in the tumor area (*SI Appendix*, Fig. S6*G*). Fig. 3*E* illustrates a representative sample with score 3. As shown in *SI Appendix*, Fig. S6*H*, most of the CRC patients had the highest score of Bv8/PROK2-positive cells.

Since Bv8/PROK2 is a secreted protein, we sought to determine whether its plasma levels have any correlation with the presence of CRC. Indeed, we found that Bv8/PROK2 levels were significantly higher in CRC patients compared with age- matched healthy donors (Fig. 4*A*). We also sought to assess whether there is a correlation between plasma Bv8/PROK2 levels and survival of CRC patients. Plasma samples were available from a total of 120 patients from the IFL (irinotecan, 5-fluorouracil, leucovorin) regimen arm of trial AVF2107 (NCT00109070) (4). As shown in Fig. 4*B*, plasma Bv8/PROK2 was associated with poor overall survival (OS). Namely, patients with higher than the median value of 38.1 pg/mL plasma Bv8/PROK2 level ($n = 68$) had a median OS of 13 mo, whereas those with lower ($n = 52$) had 17.2 mo, leading to a hazard ratio of 1.77 (95% confidence interval 1.23 to 2.55, unstratified log-rank $P < 0.01$).

In Combination with Anti-VEGF Antibody, Anti-IL17a, Anti-G-CSF, or Anti-Bv8/PROK2 Suppressed Growth of Refractory Tumors, but Not anti-CXCL13 or Anti-PD-L1. To further validate the significance of G-CSF, Bv8/PROK2, and CXCL13 on anti-VEGF therapy in refractory CRC, we treated mice with anti-IL17a, anti-G-CSF, anti-Bv8/PROK2, or anti-CXCL13 antibody, in the absence or presence of anti-VEGF, for 3 wk after CIC (Fig. 4*C*). We also administered anti-PD-L1 antibody as an additional treatment group. This is because tumor-associated neutrophils (TANs) and/or granulocytic myeloid-derived suppressor cells (MDSCs) have been reported to suppress anticancer immunity through expression of PD-L1 (33, 34). In fact, expression of tumor immune factors such as *Pd1*, *Pdl1*, *Ctla4*, *Foxp3*, and *Arg1* in CIC-associated colorectal tumor tissues from *cis-Apc/Smad4* mice was up-regulated compared to small intestinal tumor tissues, whereas *CD8a* expression was down-regulated (*SI Appendix*, Fig. S7*A*). As anticipated, IHC revealed infiltration of Foxp3-positive cells in CIC-associated colorectal tumors, whereas CD8a-positive cell infiltration was observed in small intestinal tumor tissues from the same mice (*SI Appendix*, Fig. S7*B*).

Anti-G-CSF treatment, with or without anti-VEGF, suppressed neutrophil counts in peripheral blood (*SI Appendix*, Fig. S8*A*), whereas other antibodies did not. Consistent with the above findings, 3-wk treatment with anti-VEGF alone did not reduce colorectal tumor formation in *cis-Apc/Smad4* mice with CIC (tumor number, isotype 7.2 ± 3.2 vs. anti-VEGF 6.9 ± 3.0, $P = 0.85$; tumor area, isotype 36.3 ± 15.9 vs. anti-VEGF 33.6 ± 17.4 [mm^2], $P = 0.73$, Student t test) (Fig. 4 *C–E*). Anti-IL17a, anti-G-CSF, anti-Bv8/PROK2, anti-CXCL13, or anti-PD-L1 did not show any significant effects when tested as monotherapy in both *cis-Apc/Smad4* mice (tumor number, anti-IL17a 7.9 ± 3.0, anti-G-CSF 5.6 ± 2.2, anti-Bv8/PROK2 8.6 ± 3.0, ant-CXCL13 9.7 ± 5.2, anti-PD-L1 5.9 ± 2.0; tumor area, anti-IL17a 37.8 ± 20.6, anti-G-CSF 35.1 ± 14.6, anti-Bv8/PROK2 47.5 ± 15.2, anti-CXCL13 53.4 ± 32.4, anti-PD-L1 34.9 ± 16.9 [mm^2]) and *cis-Apc/Smad4 Kras$^{G12D(CDX2)}$* mice (tumor area, anti-G-CSF 286.5 ± 57.2, anti-Bv8/PROK2 295.1 ±49.0, anti-PD-L1 237.2 ± 54.8 [mm^2]) with CIC (Fig. 4 *C–E* and *SI Appendix*, Fig. S8 *D* and *E*). However, when tested in combination with anti-VEGF to DSS-fed mice, anti-IL17a, anti-G-CSF or anti-Bv8/PROK2, but not anti-PD-L1, antibody significantly reduced the lesion areas and/or numbers of colorectal tumors *cis-Apc/Smad4* mice with CIC (tumor numbers, anti-VEGF + anti-IL17a 4.9 ± 3.8, vs. isotype $P = 0.21$, anti-VEGF + anti-G-CSF 3.4 ± 2.0, vs. isotype $P < 0.01$, anti-VEGF + anti-Bv8/PROK2 4.1 ± 2.5, vs. isotype $P < 0.01$; tumor area, anti-VEGF + anti-IL17a 17.9 ± 16.2 [mm^2], vs. isotype $P < 0.05$, anti-VEGF + anti-G-CSF 12.0 ± 9.0 [mm^2], vs. isotype $P < 0.01$, anti-VEGF + anti-Bv8/PROK2 13.6 ± 8.9 [mm^2], vs. isotype $P < 0.01$, Student's t test) (Fig. 4 *C–E*). We also confirmed that anti-G-CSF (or anti-Bv8/PROK2) neutralization in combination with anti-VEGF significantly suppressed colorectal tumor formation in *cis-Apc/Smad4 Kras$^{G12D(CDX2)}$* mice (tumor area, anti-VEGF + anti-G-CSF 165 ± 60 [mm^2], vs. isotype $P < 0.01$, anti-VEGF + anti-Bv8/PROK2 168 ± 37 [mm^2], vs. isotype $P < 0.01$, Student's t test) (*SI Appendix*, Fig. S8 *D* and *E*). These results suggest that neutralization of both VEGF and IL17a or VEGF and G-CSF/Bv8/PROK2 is required to suppress tumor formation after CIC in *cis-Apc/Smad4* mice and *cis-Apc/Smad4 Kras$^{G12D(CDX2)}$* mice. Treatment of *cis-Apc/Smad4* mice with anti-CXCL13 resulted in a trend toward increases in colorectal tumor formation. Although this increase did not fully reach statistical significance (tumor numbers, anti-CXCL13 9.7 ± 5.2, vs. isotype $P = 0.22$; anti-VEGF + anti-CXCL13 12.0 ± 4.9, vs. isotype $P = 0.02$. tumor area, anti-CXCL13 53.4 ± 32.4 [mm^2], vs. isotype $P = 0.15$; anti-VEGF + anti-CXCL13 62.2 ± 35.6 [mm^2], vs. isotype $P = 0.05$, Student's t test), we noted that some of the largest tumors in this study were in the anti-CXCL13 groups (Fig. 4 *C–E*). Remarkably, in small intestinal tumors of *cis-Apc/Smad4* mice and *cis-Apc/Smad4 Kras$^{G12D(CDX2)}$* mice with CIC, anti-VEGF monotherapy achieved significant tumor suppression (*SI Appendix*, Fig. S8 *B* and *C*).

In DSS-treated *cis-Apc/Smad4* mice receiving these combination therapies, we also confirmed neutrophil infiltration and angiogenesis in colorectal tumors by immunofluorescent staining (Fig. 5 *A* and *C*). Anti-G-CSF treatment, with or without anti-VEGF, significantly reduced neutrophil infiltration inside the tumor microenvironment, consistent with the peripheral white blood cell counts (Fig. 5 *A* and *C* and *SI Appendix*, Fig. S8*A*). Anti-IL17a and anti-Bv8/PROK2 treatment also had similar effects, suppressing local neutrophil infiltration, without significantly affecting peripheral neutrophil counts (Fig. 5 *A* and *C* and *SI Appendix*, Fig. S8*A*). Angiogenesis in the colorectal tumors was dramatically suppressed when DSS-fed *cis-Apc/Smad4* mice were treated with anti-IL17a, anti-G-CSF, or anti-Bv8/PROK2 antibody in combination with anti-VEGF (Fig. 5 *B* and *D*). In contrast, none of the monotherapies with anti-IL17a, anti-G-CSF, or anti-Bv8/PROK2 antibody caused such angiogenesis-suppressive effects inside colorectal tumors, which is consistent with the results of tumor suppression described above.

G-CSF Expression Confers Resistance to Anti-VEGF Therapy in a Mouse Allograft Model of CRC Liver Metastasis. CRC becomes lethal when it metastasizes to distant organs, the liver being the most common. Therefore, we sought to verify the above results using allograft models of CRC liver metastasis. Anti-VEGF therapy was effective when MC38 mouse CRC cells were grown in the liver of C57BL/6 syngeneic mice following injection in the spleen, as assessed by liver weight (isotype 3.5 ± 2.0 vs. anti-VEGF 1.2 ± 0.4 [g], $P < 0.05$, Student's t test) (*SI Appendix*, Fig. S9 *A* and *B*). We transduced *Gcsf* into MC38 cells (*SI Appendix*, Fig. S9*C*). Lentiviral transduction of *Gcsf* significantly increased G-CSF expression from cancer cells, leading to increased serum G-CSF

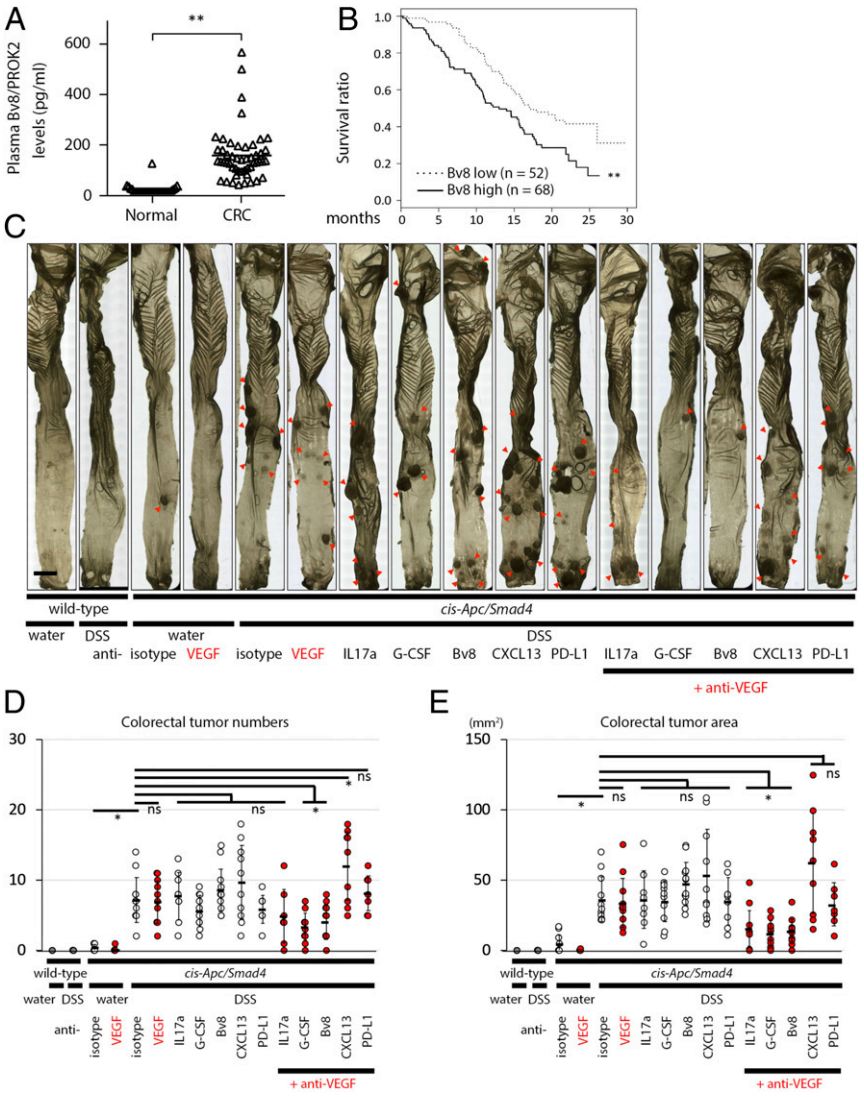

Fig. 4. Plasma Bv8/PROK2 levels and survival correlations and treatment of anti-IL17a/G-CSF/Bv8/PROK2 axis in combination with anti-VEGF in *cis-Apc/Smad4* mice with DSS. (*A*) Plasma Bv8/PROK2 levels of CRC patients and age-matched healthy volunteers. $^{**}P < 0.01$, Mann–Whitney *u* test. (*B*) Kaplan–Meier estimates of the subpopulation from the cohort of AVF2107 trial (4, 32). Patients from the IFL arm were divided into two groups, one with plasma Bv8/PROK2 levels higher than median value (= 38.1 pg/mL) and the other with lower value. $^{**}P < 0.01$, log-rank test. (*C*) Representative images of colorectum from wild-type or *cis-Apc/Smad4* mice, with or without DSS administration, followed by the indicated antibody treatments. (Scale bar, 5 mm.) Red arrowhead, colorectal tumors. (*D* and *E*) Comparison of tumor numbers (*D*) and total tumor areas (*E*) of *cis-Apc/Smad4* mice with DSS, followed by indicated antibody treatments. $n = 8, 8, 10, 9, 11, 11, 8, 10, 12, 10, 8, 7, 11, 11, 9$, and 7 in group from the *Left*. $^{*}P < 0.05$; ns, not significant, Student's *t* test.

levels and recruitment of polynuclear neutrophils expressing Bv8 in liver metastatic foci (Fig. 6*B* and *SI Appendix*, Fig. S9*D*). Importantly, G-CSF expressing MC38 cells acquired resistance to anti-VEGF (MC38-empty 1.1 ± 0.17 vs. MC38-Gcsf 1.54 ± 0.58 [g], $P < 0.05$, Student's *t* test) (Fig. 6*A*), and neutralization of G-CSF/Bv8 cascade with anti-G-CSF/anti-Bv8 antibodies in combination with anti-VEGF abrogated the acquired resistance in G-CSF-expressing tumors (isotype 1.9 ± 0.93 [g], anti-VEGF + anti-G-CSF 1.0 ± 0.25, vs. isotype $P < 0.05$; anti-VEGF + anti-Bv8 0.97 ± 0.18, vs. isotype $P < 0.05$, Student's *t* test) (Fig. 6*C*). The treatments including anti-G-CSF antibody suppressed peripheral neutrophil counts in this model, whereas other treatments did not (Fig. 6*D*). Another CRC metastasis allograft model with CT26 cells derived from BALB/c mouse showed essentially the same results (*SI Appendix*, Fig. S9 *E–H*).

We established a spontaneous liver metastasis model in accordance with a previous report, with minor modifications (35). As expected, mice with $Kras^{+/LSL\text{-}G12D}$ and $Pten^{flox/flox}$ transgene driven by *villin-Cre* ($Kras^{G12D}$ $Pten^{flox/flox}$) showed both intestine and liver tumors (Fig. 6 *E–G*). We confirmed that liver tumors in this mouse model derived from intestinal epithelial cells by adding $Gt(ROSA26)^{ACTB\text{-}tdTomato\text{-}EGFP}$ gene (Fig. 6 *F* and *G* and *SI Appendix*, Fig. S9*I*). As reported, both intestinal primary tumor and liver metastasis tumors showed Wnt and Erk activation in cancer cells, which is a common feature of advanced CRC (*SI Appendix*, Fig. S9*J*) (35). Metastatic liver tumors in this model demonstrated prominent up-regulation of *Csf3* and *Prok2* expression, and histological examination revealed significant recruitment of polynuclear neutrophils with Bv8/PROK2 expression in the liver tumors (Fig. 6 *H* and *I*). Collectively, these results demonstrate that the G-CSF/Bv8/PROK2 axis played an important role in eliciting resistance to anti-VEGF therapy for CRC liver metastasis, and that blockade of G-CSF/Bv8/PROK2 can become a therapeutic target for such tumors.

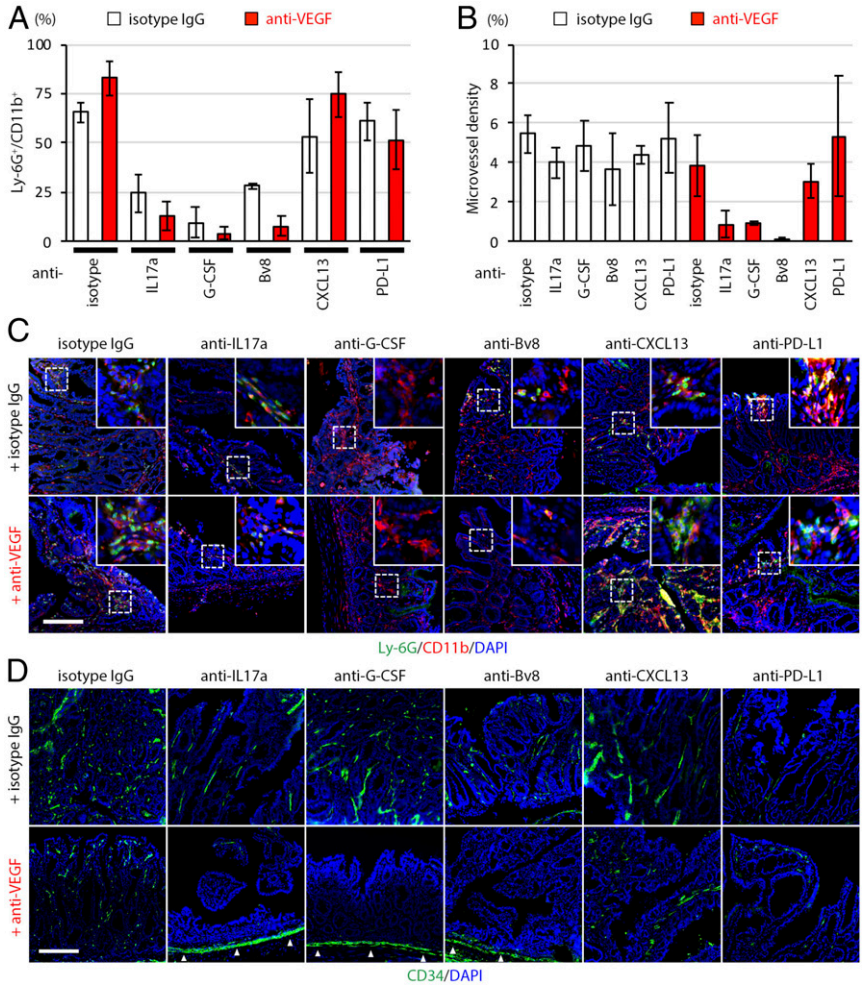

Fig. 5. Neutrophil infiltration and microvascular development in the stroma of CIC-associated colorectal tumors. (*A*) Quantification of Ly-6G$^+$ cells proportion within CD11b$^+$ cells inside the tumor stroma shown in C. $n = 3$ in each group. (*B*) Quantification of microvessel density within the tumor stroma shown in D. $n = 3$ in each group. (*C*) Immunofluorescent staining of Ly-6G (green) and CD11b (red) cells in colorectal tumor tissues of *cis-Apc/Smad4* mice with DSS followed by indicated treatment. (Scale bar, 200 μm.) (*D*) Immunofluorescent staining of CD34 (green) in colorectal tumor tissue of *cis-Apc/Smad4* mice with DSS followed by indicated treatment. (Scale bar, 200 μm.) White arrowhead, major vessels in muscle layer.

Discussion

We investigated the mechanisms of resistance to anti-VEGF in GEMMs of CRC and evaluated their relevance to clinical outcomes in human patients. In our mouse models, administration of anti-Bv8/PROK2, anti-G-CSF, or anti-IL17a antibody in combination with anti-VEGF effectively suppressed colorectal tumor formation on GEMM with CIC, although anti-IL17a antibody appeared slightly less effective than the other treatment groups. In the clinical setting, bevacizumab is typically used in combination with cytotoxic chemotherapy agents that typically cause neutropenia. Anti-G-CSF antibody may exacerbate chemotherapy-induced neutropenia, which may cause critical infectious diseases. Moreover, in addition to G-CSF, GM-CSF and IL10 can also stimulate Bv8/PROK2 expression in human neutrophils/monocytes (36). On the other hand, Bv8/PROK2 is a downstream target of G-CSF (30), and anti-Bv8/PROK2 treatment did not cause neutropenia in our mouse model (Fig. 6*D* and *SI Appendix*, Fig. S8*A*). Therefore, targeting Bv8/PROK2 may be a safer approach.

We found a biphasic increase in serum G-CSF levels after treatment with DSS in *cis-Apc/Smad4* mice (Fig. 2*F*). The initial peak was observed almost immediately after DSS exposure, both in *cis-Apc/Smad4* and wild-type mice, which may have been caused by the acute inflammation. However, DSS-treated *cis-Apc/Smad4*, but not DSS-treated wild-type mice, showed a gradual increase in serum G-CSF levels, with or without anti-VEGF treatment. These increased G-CSF levels were accompanied by colorectal tumor growth (Fig. 2*F*). The main source of this secondary G-CSF peak was the tumor tissue itself (Fig. 3*A*), suggesting that tumor-derived G-CSF played an important role in recruiting neutrophils (TAN and/or granulocytic-MDSC) to the tumor site. The spontaneous liver metastasis model with *Kras*^{G12D} *Pten*$^{flox/flox}$ also revealed that G-CSF expression from metastatic tumors was associated with recruitment of neutrophils at the metastatic sites. It is believed that neutrophils play an important role in tumorigenesis for many types of cancers, although their role is complex and possibly tumor dependent and may result in tumor promotion or suppression (37, 38). For example, a high preoperative neutrophil-to-lymphocyte ratio (NLR) from peripheral blood cell counts has been correlated with overall survival in CRC (39) or in other types of cancers (40, 41). Recent studies reported that NLR may predict chemotherapy outcomes in advanced cancers (42, 43). NLR has been also reported to predict benefit from bevacizumab therapy in patients with advanced CRC (44, 45). In addition to systemic neutrophils as a marker of inflammatory, neutrophilic/granulocytic lineage cells inside the tumor microenvironment such as TAN or their precursors,

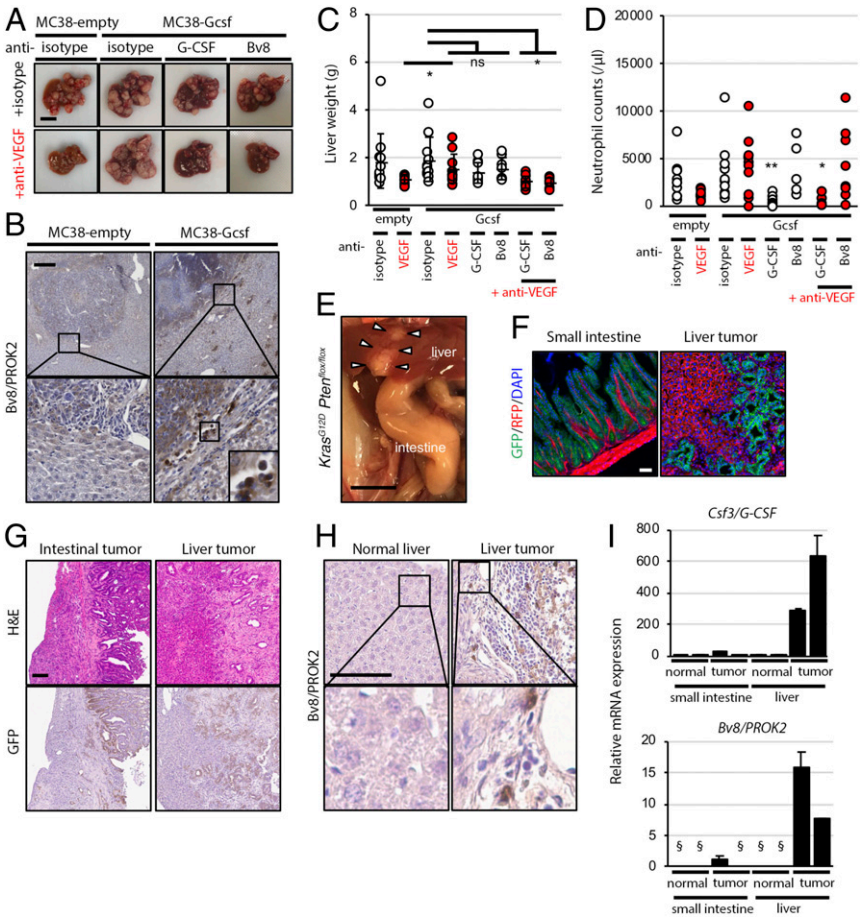

Fig. 6. G-CSF-expressing CRC liver metastasis acquired resistance to anti-VEGF treatment, and neutralization of G-CSF/Bv8 signaling abrogated it. (*A*) Representative images of MC38 liver metastasis following treatment with indicated neutralizing antibodies. (Scale bar, 1 cm.) (*B*) IHC for Bv8/PROK2 in tumor tissues of MC38 liver metastasis with or without G-CSF expression. (Scale bar, 200 μm.) (*C*) Comparison of liver weights from MC38 liver metastasis model treated with indicated neutralizing antibodies. n = 11, 11, 11, 11, 8, 8, 8, 8, respectively, in each group. $*P < 0.05$. ns, not significant, Student's t test. (*D*) Neutrophil counts of peripheral blood from mice with liver metastasis and indicated treatment. n = 11, 11, 11, 11, 8, 8, 8, 8, respectively, in each group. $**P < 0.01$, $*P < 0.05$ compared to MC38-Gcsf with isotype treatment, Mann–Whitney u test. (*E*) Representative picture of liver and intestine in *villin-Cre* $Kras^{G12D}$ $Pten^{flox/flox}$ $Gt(ROSA26)^{ACTB\text{-}tdTomato\text{-}EGFP}$ mouse. White arrowheads, liver tumor. (Scale bar, 1 cm.) (*F*) Pictures of intestine and liver with tumor from a *villin-Cre* $Kras^{G12D}$ $Pten^{flox/flox}$ $Gt(ROSA26)^{ACTB\text{-}tdTomato\text{-}EGFP}$ mouse taken by fluorescent microscope. (Scale bar, 50 μm.) (*G*) Histopathology and indicated IHC of intestine and liver tumors from a *villin-Cre* $Kras^{G12D}$ $Pten^{flox/flox}$ $Gt(ROSA26)^{ACTB\text{-}tdTomato\text{-}EGFP}$ mouse. (Scale bar, 100 μm.) (*H*) IHC of normal liver and liver tumor for Bv8/PROK2 in a *villin-Cre* $Kras^{G12D}$ $Pten^{flox/flox}$ $Gt(ROSA26)^{ACTB\text{-}tdTomato\text{-}EGFP}$ mouse. *Lower* are magnification showing polynuclear granulocytes. (Scale bar, 100 μm.) (*I*) Relative mRNA expression of *Csf3* and *Bv8/PROK2* from normal and tumor tissues of intestine and liver in *villin-Cre* $Kras^{G12D}$ $Pten^{flox/flox}$ $Gt(ROSA26)^{ACTB\text{-}tdTomato\text{-}EGFP}$ mice. Experiments were repeated three times. §, undetectable level.

granulocytic MDSCs, are also thought to play a major role in tumor immunity (46). However, it is as yet unclear whether neutrophils inside the tumor microenvironment promote or suppress tumor progression (37). In fact, while some of the previous clinical reports showed that presence of neutrophils inside tumors was an independent poor prognostic factor for several types of cancers (34, 47), others showed that neutrophils can play antitumoral roles (48).

IL17a, mainly produced by Th17 helper lymphocytes, is one of the key players of inflammation, including inflammatory bowel disease (IBD). In addition to IBD, IL17a plays a critical role in the pathogenesis of colitis-associated cancers (49). In the present study, we demonstrated that IL17a stimulate G-CSF expression from cancer cells, which recruits neutrophils in the tumor microenvironment. Among several possible explanations of how neutrophils promote tumor growth, angiogenesis represents an attractive possibility (37, 50). We have previously reported that tumor-infiltrating $CD11b^{+}Gr\text{-}1^{+}$ cells with neutrophilic/granulocytic phenotype produced the Bv8/PROK2 protein, which resulted in refractoriness to anti-VEGF therapy (29, 51, 52). However, most of these studies were performed in tumor allograft/xenograft models that may not accurately reflect the complexity of the tumor microenvironment.

In the present study, we used CIC to stimulate colonic tumorigenesis in an intestinal cancer GEMM (*cis-Apc*/*Smad4* and *cis-Apc*/*Smad4* $Kras^{G12D(CDX2)}$). Colorectal tumors with CIC and metastatic liver tumors in our models contained abundant neutrophils in their stroma, which also reflects human CRC (48). Without DSS, *cis-Apc*/*Smad4* mice showed tumors mainly in small intestine, and they received a marked benefit from anti-VEGF therapy. On the other hand, DSS-treated *cis-Apc*/*Smad4* mice developed tumors also in the colorectum that showed resistance to anti-VEGF antibody, suggesting that CIC triggered escape mechanisms. Interestingly, even in DSS-treated *cis-Apc*/*Smad4* mice and *cis-Apc*/*Smad4* $Kras^{G12D(CDX2)}$ mice, small intestinal tumors were still responsive to anti-VEGF therapy (Fig. 2*C* and *SI Appendix*, Fig. S8 *B* and *C*), suggesting that inflammation is important for resistance to antiangiogenesis since DSS causes inflammation primarily in the colon (*SI Appendix*, Figs. S3*B* and S4*A*). These findings raise the possibility that heterogeneity in the tumor responses to anti-VEGF may be, at

least in part, related to different degrees of inflammation in different regions/sites, even within the same tumor. To identify factors potentially implicated in such resistance, we focused our analysis on serum samples because systemically released factors are likely implicated in the recruitment of inflammatory cells from the bone marrow or the systemic circulation into the inflamed colon. Analysis of mouse sera by cytokine arrays demonstrated that only G-CSF and CXCL13 were significantly elevated in DSS-treated mice compared to controls (*SI Appendix*, Fig. S5 *A* and *D*). As for CXCL13, it was increased also in the DSS-treated wild-type mice that never showed intestinal tumors, arguing against a role of this chemokine in tumor growth (Fig. 2*G*). CXCL13 is a CXC chemokine originally implicated in the recruitment and development of B cells through interaction with CXCR5 (53). The significance of CXCL13 in tumor biology has been somewhat controversial. Bindea et al. reported that patients with high CXCL13 expression in colorectal cancer show better survival than those with low expression (54) and hypothesized that CXCL13 plays an important role in anticancer immunity. However, other studies have reported a stimulatory role of CXCL13 for various tumor cell types, including colorectal cancer cells (55, 56), raising the possibility that this chemokine may be a therapeutic target in cancer. Our findings seem consistent with the hypothesis that CXCL13 represents a homeostatic mechanism limiting tumor growth (54) since tumors in anti-CXCL13-treated groups tended to be the largest.

Anti-PD-L1 antibody treatment, with or without anti-VEGF, did not cause tumor suppression, which is consistent with the lack of clinical efficacy in CRC patients without MSI (13). Interestingly, combination of an anti-PD-L1 antibody with bevacizumab has yielded promising results in multiple malignancies (57–59), but there are no reports that such combination enhances the efficacy of bevacizumab in CRC.

There are four consensus molecular subtypes (CMSs) of CRC (60). Among these, CMS4, with activation of TGF-β and angiogenesis, predicts the worst prognosis. The CIC CRC mouse models we used here may truly reflect the clinical setting of aggressive CMS4 CRC, because CRC tissues from *cis-Apc/Smad4* mice showed up-regulation of *Tgfb1* and some angiogenic factors such as *Bv8/PROK2* and *Plgf* (*SI Appendix*, Fig. S4*B*). In addition, it was reported that serum G-CSF levels are strongly correlated with tumor stage in colorectal cancer patients (31). Further evidence for the CRC mouse models reflecting real clinical setting comes from the high frequency of Bv8/PROK2-positive neutrophils observed in human CRC (Fig. 4*A* and *SI Appendix*, Fig. S6*H*). Moreover, plasma Bv8/PROK2 levels were associated with poor prognosis in this disease, providing a potential strategy to target Bv8/PROK2 as a suitable candidate for therapeutic intervention. We used *cis-Apc/Smad4* mice as the CIC CRC model because expression profile from tumor tissues of either $Apc^{\Delta 716}$, *cis-Apc/Smad4*, or *cis-Apc/Smad4* $Kras^{G12D(CDX2)}$ essentially showed little difference between each other (*SI Appendix*, Fig. S4*C*).

We also found that liver tumors in a spontaneous metastasis model with $Kras^{G12D}$ $Pten^{flox/flox}$ driven by *villin-Cre* transgene showed significant increases in *Csf3* and *Bv8/Prok2* expression (Fig. 6*I*). We did not attempt to treat these mice with targeted antibodies since it has been reported that the frequency of liver metastasis is only 25%, and that some of the metastases take over 1 y to be detectable (35). Therefore, it could be challenging to generate statistically significant data in a timely fashion. Nevertheless, this model provides support for our hypothesis as it shows that metastatic foci in the liver express abundant amounts of G-CSF, with recruitment of Bv8-expressing polynuclear granulocytes.

In conclusion, on the basis of the GEMM findings reported in this manuscript, we provide a validation of the potential role for the G-CSF/Bv8/PROK2 axis as a therapeutic target in human colorectal cancer. A challenge in developing anti-Bv8 therapy was the difficulty in identifying an antibody that fully blocked Bv8 function, hence the need to combine two antibodies, in this and in earlier studies (29, 52). Hopefully, our findings will renew interest in developing reagents more suitable for clinical trials.

Materials and Methods

Cytokine Array. Serum samples were diluted 10-fold and applied to the membranes of Mouse Cytokine Array Panel A (R&D Systems), according to the manufacturer's protocol. After incubation with biotinylated detection antibody mixture, membranes were treated with streptavidin-conjugated IRDye800CW (LI-COR Biosciences), and fluorescent intensity was detected by Odyssey (LI-COR).

Quantitative Reverse Transcription PCR (qRT-PCR). Total RNA was extracted using RNeasy Plus Mini Kit (Qiagen) according to the manufacturer's protocol. cDNA was generated using High Capacity cDNA Reverse Transcription Kit (Applied Biosystems), followed by quantification with TaqMan Fast Advanced Master Mix (Thermo Fisher Scientific) using ViiA 7 (Applied Biosystems). Expression levels for mouse genes listed in *SI Appendix*, Supplementary Table were normalized by mouse *Actb*. The ΔΔCt method was used for quantification of gene expression levels.

ELISA. Mouse sera were diluted fivefold, and G-CSF and CXCL13 levels were measured using specific ELISA kits (MCS00 and MCX130 respectively, R&D Systems). For G-CSF ELISA in conditioned media of mouse CRC cell lines, 1.0×10^5 cells were seeded in six-well plates with 1 mL of Dulbecco's Modified Eagle Medium containing 10% fetal bovine serum, and cultured for 24 h. The absorbance was measured at 450 nm using the plate reader SpectraMax M5 (Molecular Devices). For human Bv8/PROK2, assay plates were coated with anti-Bv8/PROK2 antibody (1 μg/mL, clone 3B8) at 4 °C overnight, and after a brief wash with wash buffer (0.05% Tween-20 in phosphate-buffered saline), human plasma samples were applied and incubated for 2 h. Anti-Bv8/PROK2 (clone 3F1) was used as detection antibody. Animal studies were approved and performed in compliance with guidelines by the University of California San Diego (UCSD) Institutional Animal Care and Use Committee.

Data Availability. All data are included in the article and supporting information.

ACKNOWLEDGMENTS. Antibodies targeting VEGF-A, Bv8/PROK2, IL17a, and PD-L1 were kindly provided by Genentech, Inc. We are grateful to Franklin Peale for Bv8/PROK2 IHC in human tumors. We thank J. Silvio Gutkind for a reporter mouse; Fumihiko Kakizaki and David R. Vera for helpful discussions and logistic support; Wei Liang for providing mouse tumor tissues; Rosemary Bai for help with mouse colony maintenance; Wataru Hirata, Hiroyuki Miyoshi, and Yoshiharu Sakai for help with CRC spheroid culture; and Ryosuke Okamura for help with statistical analyses.

1. N. Ferrara, A. P. Adamis, Ten years of anti-vascular endothelial growth factor therapy. *Nat. Rev. Drug Discov.* **15**, 385–403 (2016).
2. R. S. Apte, D. S. Chen, N. Ferrara, VEGF in signaling and disease: Beyond discovery and development. *Cell* **176**, 1248–1264 (2019).
3. G. C. Jayson, R. Kerbel, L. M. Ellis, A. L. Harris, Antiangiogenic therapy in oncology: Current status and future directions. *Lancet* **388**, 518–529 (2016).
4. H. Hurwitz *et al*., Bevacizumab plus irinotecan, fluorouracil, and leucovorin for metastatic colorectal cancer. *N. Engl. J. Med.* **350**, 2335–2342 (2004).
5. B. J. Giantonio *et al*.; Eastern Cooperative Oncology Group Study E3200, Bevacizumab in combination with oxaliplatin, fluorouracil, and leucovorin (FOLFOX4) for previously treated metastatic colorectal cancer: Results from the eastern cooperative oncology group study E3200. *J. Clin. Oncol.* **25**, 1539–1544 (2007).
6. J. Bennouna *et al*.; ML18147 Study Investigators, Continuation of bevacizumab after first progression in metastatic colorectal cancer (ML18147): A randomised phase 3 trial. *Lancet Oncol.* **14**, 29–37 (2013).
7. R. S. Kerbel, Tumor angiogenesis. *N. Engl. J. Med.* **358**, 2039–2049 (2008).
8. M. Potente, H. Gerhardt, P. Carmeliet, Basic and therapeutic aspects of angiogenesis. *Cell* **146**, 873–887 (2011).
9. M. R. Junttila, F. J. de Sauvage, Influence of tumour micro-environment heterogeneity on therapeutic response. *Nature* **501**, 346–354 (2013).
10. Y. Itatani *et al*., The role of chemokines in promoting colorectal cancer invasion/metastasis. *Int. J. Mol. Sci.* **17**, 643 (2016).
11. J. Galon *et al*., Cancer classification using the immunoscore: A worldwide task force. *J. Transl. Med.* **10**, 205 (2012).
12. J. R. Brahmer *et al*., Safety and activity of anti-PD-L1 antibody in patients with advanced cancer. *N. Engl. J. Med.* **366**, 2455–2465 (2012).
13. D. T. Le *et al*., PD-1 blockade in tumors with mismatch-repair deficiency. *N. Engl. J. Med.* **372**, 2509–2520 (2015).
14. C. R. Boland, A. Goel, Microsatellite instability in colorectal cancer. *Gastroenterology* **138**, 2073–2087.e3 (2010).

15. J. Terzić, S. Grivennikov, E. Karin, M. Karin, Inflammation and colon cancer. *Gastroenterology* **138**, 2101–2114.e5 (2010).
16. N. Korsisaari *et al*., Inhibition of VEGF-A prevents the angiogenic switch and results in increased survival of Apc+/min mice. *Proc. Natl. Acad. Sci. U.S.A.* **104**, 10625–10630 (2007).
17. L. K. Su *et al*., Multiple intestinal neoplasia caused by a mutation in the murine homolog of the APC gene. *Science* **256**, 668–670 (1992).
18. K. Takaku *et al*., Intestinal tumorigenesis in compound mutant mice of both Dpc4 (Smad4) and Apc genes. *Cell* **92**, 645–656 (1998).
19. W. C. Liang *et al*., Cross-species vascular endothelial growth factor (VEGF)-blocking antibodies completely inhibit the growth of human tumor xenografts and measure the contribution of stromal VEGF. *J. Biol. Chem.* **281**, 951–961 (2006).
20. D. A. Tuveson *et al*., Endogenous oncogenic K-ras(G12D) stimulates proliferation and widespread neoplastic and developmental defects. *Cancer Cell* **5**, 375–387 (2004).
21. B. B. Madison *et al*., Cis elements of the villin gene control expression in restricted domains of the vertical (crypt) and horizontal (duodenum, cecum) axes of the intestine. *J. Biol. Chem.* **277**, 33275–33283 (2002).
22. A. Mantovani, P. Allavena, A. Sica, F. Balkwill, Cancer-related inflammation. *Nature* **454**, 436–444 (2008).
23. J. Burn *et al*.; CAPP2 Investigators, Long-term effect of aspirin on cancer risk in carriers of hereditary colorectal cancer: An analysis from the CAPP2 randomised controlled trial. *Lancet* **378**, 2081–2087 (2011).
24. H. S. Cooper *et al*., The role of mutant Apc in the development of dysplasia and cancer in the mouse model of dextran sulfate sodium-induced colitis. *Gastroenterology* **121**, 1407–1416 (2001).
25. Y. Feng *et al*., Sox9 induction, ectopic Paneth cells, and mitotic spindle axis defects in mouse colon adenomatous epithelium arising from conditional biallelic Apc inactivation. *Am. J. Pathol.* **183**, 493–503 (2013).
26. S. Kitajima, S. Takuma, M. Morimoto, Tissue distribution of dextran sulfate sodium (DSS) in the acute phase of murine DSS-induced colitis. *J. Vet. Med. Sci.* **61**, 67–70 (1999).
27. A. S. Chung *et al*., An interleukin-17-mediated paracrine network promotes tumor resistance to anti-angiogenic therapy. *Nat. Med.* **19**, 1114–1123 (2013).
28. H. Miyoshi, T. S. Stappenbeck, In vitro expansion and genetic modification of gastrointestinal stem cells in spheroid culture. *Nat. Protoc.* **8**, 2471–2482 (2013).
29. F. Shojaei *et al*., Bv8 regulates myeloid-cell-dependent tumour angiogenesis. *Nature* **450**, 825–831 (2007).
30. L. Negri, N. Ferrara, The prokineticins: Neuromodulators and mediators of inflammation and myeloid cell-dependent angiogenesis. *Physiol. Rev.* **98**, 1055–1082 (2018).
31. B. Mroczko *et al*., The diagnostic value of G-CSF measurement in the sera of colorectal cancer and adenoma patients. *Clin. Chim. Acta* **371**, 143–147 (2006).
32. A. Grothey *et al*., Response-independent survival benefit in metastatic colorectal cancer: A comparative analysis of N9741 and AVF2107. *J. Clin. Oncol.* **26**, 183–189 (2008).
33. M. Z. Noman *et al*., PD-L1 is a novel direct target of HIF-1α, and its blockade under hypoxia enhanced MDSC-mediated T cell activation. *J. Exp. Med.* **211**, 781–790 (2014).
34. T.-T. Wang *et al*., Tumour-activated neutrophils in gastric cancer foster immune suppression and disease progression through GM-CSF-PD-L1 pathway. *Gut* **66**, 1900–1911 (2017).
35. E. J. Davies, V. Marsh Durban, V. Meniel, G. T. Williams, A. R. Clarke, PTEN loss and KRAS activation leads to the formation of serrated adenomas and metastatic carcinoma in the mouse intestine. *J. Pathol.* **233**, 27–38 (2014).
36. C. Zhong, X. Qu, M. Tan, Y. G. Meng, N. Ferrara, Characterization and regulation of bv8 in human blood cells. *Clin. Cancer Res.* **15**, 2675–2684 (2009).
37. W. Liang, N. Ferrara, The complex role of neutrophils in tumor angiogenesis and metastasis. *Cancer Immunol. Res.* **4**, 83–91 (2016).
38. W. Liang, Q. Li, N. Ferrara, Metastatic growth instructed by neutrophil-derived transferrin. *Proc. Natl. Acad. Sci. U.S.A.* **115**, 11060–11065 (2018).
39. S. R. Walsh, E. J. Cook, F. Goulder, T. A. Justin, N. J. Keeling, Neutrophil-lymphocyte ratio as a prognostic factor in colorectal cancer. *J. Surg. Oncol.* **91**, 181–184 (2005).
40. K. M. Sarraf *et al*., Neutrophil/lymphocyte ratio and its association with survival after complete resection in non-small cell lung cancer. *J. Thorac. Cardiovasc. Surg.* **137**, 425–428 (2009).
41. M. Stotz *et al*., Increased neutrophil-lymphocyte ratio is a poor prognostic factor in patients with primary operable and inoperable pancreatic cancer. *Br. J. Cancer* **109**, 416–421 (2013).
42. I. R. Cho *et al*., Pre-treatment neutrophil to lymphocyte ratio as a prognostic marker to predict chemotherapeutic response and survival outcomes in metastatic advanced gastric cancer. *Gastric Cancer* **17**, 703–710 (2014).
43. W. Chua, K. A. Charles, V. E. Baracos, S. J. Clarke, Neutrophil/lymphocyte ratio predicts chemotherapy outcomes in patients with advanced colorectal cancer. *Br. J. Cancer* **104**, 1288–1295 (2011).
44. V. Formica *et al*., Systemic inflammation, as measured by the neutrophil/lymphocyte ratio, may have differential prognostic impact before and during treatment with fluorouracil, irinotecan and bevacizumab in metastatic colorectal cancer patients. *Med. Oncol.* **31**, 166 (2014).
45. A. Passardi *et al*., Inflammatory indexes as predictors of prognosis and bevacizumab efficacy in patients with metastatic colorectal cancer. *Oncotarget* **7**, 33210–33219 (2016).
46. D. I. Gabrilovich, Myeloid-derived suppressor cells. *Cancer Immunol. Res.* **5**, 3–8 (2017).
47. Y. Ino *et al*., Immune cell infiltration as an indicator of the immune microenvironment of pancreatic cancer. *Br. J. Cancer* **108**, 914–923 (2013).
48. V. Governa *et al*., The interplay between neutrophils and $CD8^+$ T cells improves survival in human colorectal cancer. *Clin. Cancer Res.* **23**, 3847–3858 (2017).
49. Y. S. Hyun *et al*., Role of IL-17A in the development of colitis-associated cancer. *Carcinogenesis* **33**, 931–936 (2012).
50. S. B. Coffelt, M. D. Wellenstein, K. E. de Visser, Neutrophils in cancer: Neutral no more. *Nat. Rev. Cancer* **16**, 431–446 (2016).
51. F. Shojaei *et al*., Tumor refractoriness to anti-VEGF treatment is mediated by CD11b+Gr1+ myeloid cells. *Nat. Biotechnol.* **25**, 911–920 (2007).
52. M. Kowanetz *et al*., Granulocyte-colony stimulating factor promotes lung metastasis through mobilization of Ly6G+Ly6C+ granulocytes. *Proc. Natl. Acad. Sci. U.S.A.* **107**, 21248–21255 (2010).
53. D. F. Legler *et al*., B cell-attracting chemokine 1, a human CXC chemokine expressed in lymphoid tissues, selectively attracts B lymphocytes via BLR1/CXCR5. *J. Exp. Med.* **187**, 655–660 (1998).
54. G. Bindea *et al*., Spatiotemporal dynamics of intratumoral immune cells reveal the immune landscape in human cancer. *Immunity* **39**, 782–795 (2013).
55. J. Panse *et al*., Chemokine CXCL13 is overexpressed in the tumour tissue and in the peripheral blood of breast cancer patients. *Br. J. Cancer* **99**, 930–938 (2008).
56. Z. Zhu *et al*., CXCL13-CXCR5 axis promotes the growth and invasion of colon cancer cells via PI3K/AKT pathway. *Mol. Cell. Biochem.* **400**, 287–295 (2015).
57. J. J. Wallin *et al*., Atezolizumab in combination with bevacizumab enhances antigen-specific T-cell migration in metastatic renal cell carcinoma. *Nat. Commun.* **7**, 12624 (2016).
58. M. A. Socinski *et al*.; IMpower150 Study Group, Atezolizumab for first-line treatment of metastatic nonsquamous NSCLC. *N. Engl. J. Med.* **378**, 2288–2301 (2018).
59. R. S. Finn *et al*.; IMbrave150 Investigators, Atezolizumab plus bevacizumab in unresectable hepatocellular carcinoma. *N. Engl. J. Med.* **382**, 1894–1905 (2020).
60. J. Guinney *et al*., The consensus molecular subtypes of colorectal cancer. *Nat. Med.* **21**, 1350–1356 (2015).